Electronic Supplementary Material (ESI) for Journal of Materials Chemistry A.

Supporting Information

Arene-Perfluoroarene Interactions in Molecular Cocrystal for Enhanced Photocatalytic Activity

Lingsong Wang[a], Jingheng Deng[c], Mengjia Jiang[a], Chun Zhen[a], Fei Li[b], Shuyu Li[b], Shuming Bai[c*], Xiaotao Zhang[b*], Weigang Zhu[a*]

[a] Key Laboratory of Organic Integrated Circuits, Ministry of Education, Tianjin Key Laboratory of Molecular Optoelectronic Sciences, Department of Chemistry, School of Science, Tianjin University, Tianjin 300072, China

[b] Key Laboratory of Organic Integrated Circuits, Ministry of Education, Tianjin Key Laboratory of Molecular Optoelectronic Sciences, Institute of Molecular Aggregation Science, Tianjin University, Tianjin 300072, China

[c] Beijing National Laboratory for Molecular Sciences, State Key Laboratory for Structural Chemistry of Unstable and Stable Species, Institute of Chemistry, Chinese Academy of Sciences, Beijing 100190, China

Table of Contents

1. Reagents and materials..........S4

2. Photoluminescence Microscopy..........S5

Fig. S1. Optical and fluorescent images of micro-nano crystals.

3. Scanning Electron Microscopy..........S6

Fig. S2. Morphology and size of materials involved in photocatalytic reactions.

4. Single Crystal X-ray Diffraction..........S7

Table S1. Crystal data and structure refinement for OFN-DMA.

Fig. S3. Distance between donor and acceptor molecules.

5. Powder X-ray Diffraction..........S9

Fig. S4. Powder XRD pattern of cocrystals.

6. FTIR Spectroscopy..........S10

Fig. S5. FTIR spectrum of cocrystal and monomer.

7. UV-Vis Absorption and Photoluminescence Spectroscopy..........S11

Fig. S6. Stokes shift values of cocrystal.

Fig. S7. Tauc plots for the band gap energy.

8. Photocatalytic Measurements..........S13

Fig. S8. Power of Xe lamp used for photocatalytic experiment.

8.1. Effects of Catalyst Concentration

Fig. S9. The effect of different OFN-DMA concentrations on catalytic performance.

Fig. S10. The effect of different OFN-Pe concentrations on catalytic performance.

Fig. S11. Relationship between different concentrations and catalytic performance.

8.2. Brunauer Emmett Teller (BET) measurements and Specific Activity

Table S2. The specific activity per unit area of P25, g-C_3N_4, and OFN-Pe.

8.3. Cyclic Stability

Fig. S12. PXRD and SEM compared before and after degradation.

8.4. Universal Analysis of Photocatalysis

Fig. S13. The photocatalytic degradation performance of TC.

Fig. S14. The photocatalytic degradation performance of MB.

Table S3. Comparison of pollutant degradation performance of different organic catalysts.

9. Ultraviolet Photoelectron Spectroscopy (UPS)..........S23

Fig. S15. UPS energy spectrum of monomeric molecules.

Table S4. Summary HOMO, LUMO and bandgap, calculated from UPS spectra and UV-vis spectra.

10. Active Species Testing S25

Fig. S16. Photocatalytic degradation of RhB under different conditions.

11. Electron Paramagnetic Resonance (EPR) Spectroscopy S26

Fig. S17. EPR spectra for the detection of ·OH.

12. Atomic Force Microscopy (AFM) S27

Fig. S18. Contact potential difference profiles of cocrystals.

Fig. S19. Contact potential difference profiles (top) and surface potential images (bottom).

13. Time-resolved fluorescence spectroscopy S29

Fig. S20. Fluorescence decay curves.

Table S5. Fluorescence decay lifetime of monomers and cocrystals.

14. Electrochemical Impedance Spectroscopy (EIS) S31

Table S6. Charge transfer resistance of monomers and cocrystals.

15. Computation of Intermolecular Electronic Couplings S32

Table S7. The calculated electron and hole transfer couplings of the molecular dimers from the monocrystal of OFN.

Table S8. The calculated electron and hole transfer couplings of the molecular dimers from the monocrystal of DMA.

Table S9. The calculated electron and hole transfer couplings of the molecular dimers from the monocrystal of Pe.

Table S10. The calculated electron and hole transfer couplings of the molecular dimers from the cocrystal of OFN-DMA.

Table S11. The calculated electron and hole transfer couplings of the molecular dimers from the cocrystal of OFN-Pe.

16. References S37

1. Reagents and materials

Octafluoronaphthalene (OFN, CAS: 313-72-4, 98 %) was purchased from TCI Co.; Perylene (Pe, CAS: 198-55-0, 98 %) was purchased from TCI Co.; 9,10-Dimethylanthracene (DMA, CAS: 781-43-1, 98 %) was purchased from Tianjin Xiensi Chemical Technology Co.; Methanol (CH_3OH, HPLC), Dichloromethane (CH_2Cl_2, HPLC) and Tetrahydrofuran (C_4H_8O, HPLC) were purchased from Tianjin Jiangtian Chemical Co.; 5,5-dimethyl-1-pyrroline N-oxide (DMPO, CAS: 3317-61-1, 98 %) was purchased from Energy Chemical Co., Ltd, China. Melamine (CAS: 108-78-1, 98%), Rhodamine B (RhB, CAS: 81-88-9, 99%), Tetracycline (TC, CAS: 60-54-8, 99%), and Methylene blue (MB, CAS: 61-73-4, 99%) were purchased from Shanghai Aladdin Bio-Chem Technology Co., Ltd; TiO_2 (P25, consist of 80% anatase phase and 20% rutile phase) was purchased from Sigma-Aldrich. All the reagents were used directly without further purification.

2. Photoluminescence Microscopy

Synthesis of micro-nano cocrystals: Micro-nano crystals of OFN-DMA and OFN-Pe were fabricated by the drop-casting method. THF solutions (1 mg mL^{-1}) of OFN-DMA and OFN-Pe were dropped on clean quartz sheets, respectively. After the solvent evaporated for about 2 h, two high quality needle-like cocrystals with different colors were visualized under optical and fluorescence microscopy.

Leica DM2700 M ortho metallurgical microscope (Tianjin Key Laboratory of Molecular Optoelectronic Sciences) was used for capturing optical images of micro-nano crystals. Leica EBQ 100-04 fluorescent power source and Hg lamp (equipped with insert filter, wavelength 340~380 nm, 100 W) were used as excitation light source to obtain fluorescent images. The LED (12 V, 15 W) illumination device with constant light intensity and color temperature was used in the system. Bright-field and fluorescent pictures were captured through high resolution HD camera connected to an external display.

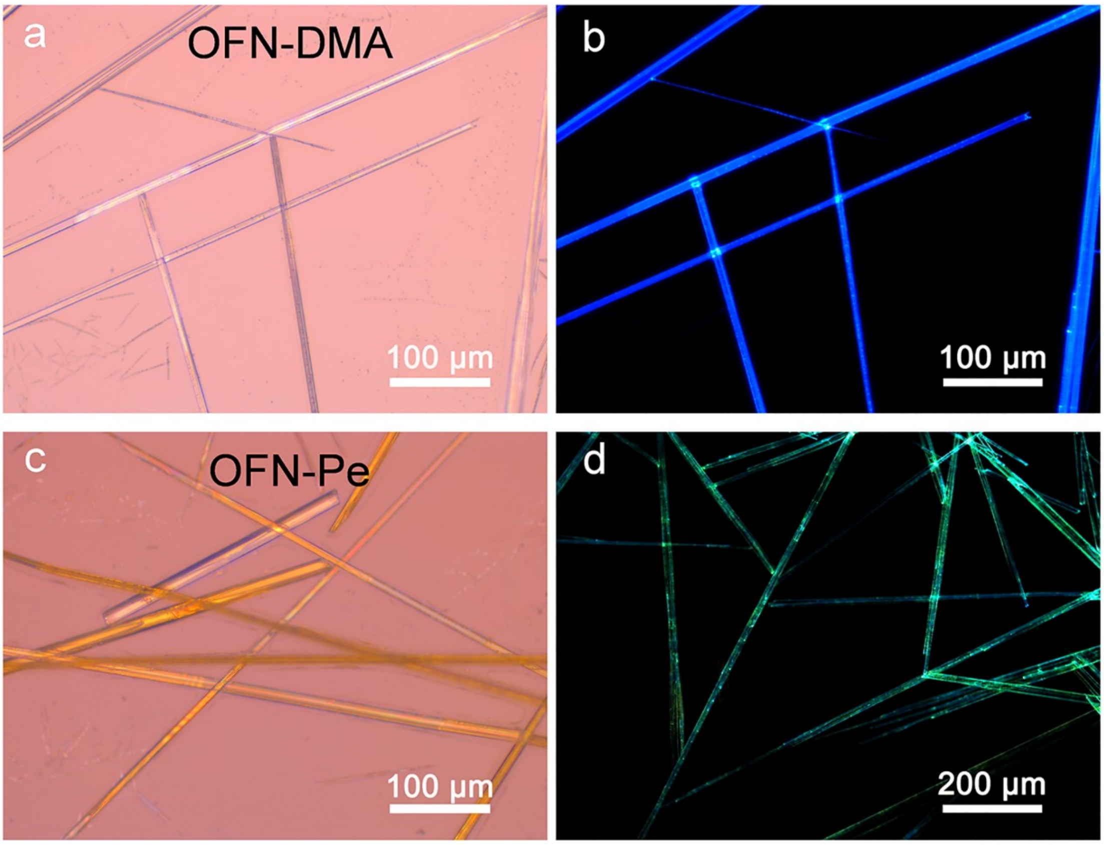

Fig. S1. Optical and fluorescent images of micro-nano crystals. (a) Optical image and (b) fluorescent image of OFN-DMA. (c) Optical image and (d) fluorescent image of OFN-Pe.

3. Scanning Electron Microscopy

The aqueous solution of catalyst (1 mg mL^{-1}) was sonicated for 10 min to obtain a uniformly dispersed solid suspension. 40 µL of the above solution was dropped on the Si/SiO_2 substrate, dried under IR lamp before morphological characterization. Field-emission scanning electron microscopy (FESEM, HITACHI UHR SU8000, Tianjin Key Laboratory of Molecular Optoelectronic Sciences) was applied to characterize the material morphology, and the acceleration voltage of the electron beam was 10 kV.

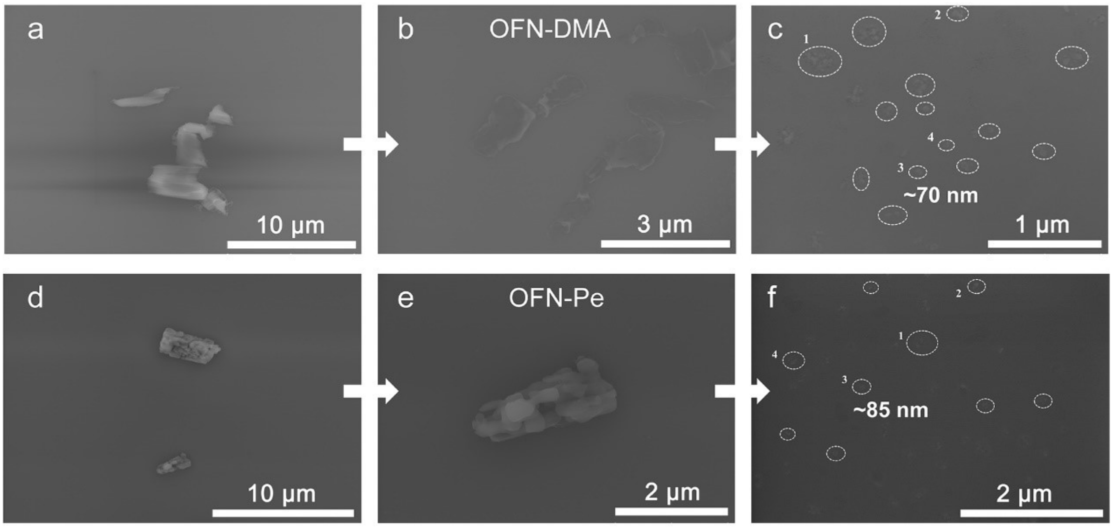

Fig. S2. Morphology and size of materials involved in photocatalytic reactions. The cocrystal powder was dispersed in water and sonicated to obtain a homogeneous dispersion for SEM characterization. (a ~ c) SEM image of OFN-DMA after ultrasound. (d ~ f) SEM image of OFN-Pe.

After ultrasonic dispersion, the morphology of cocrystals remains almost identical to solid powder. However, the dimensions of OFN-DMA and OFN-Pe change significantly after sonication. As shown in Fig. S2b and S2e, most of cocrystals are still around 3 µm in size, and a portion of the cocrystals are significantly smaller than 100 nm (Fig. S2c and S2f). As can be noticed from the SEM images, the cocrystal sizes involved in the catalytic reaction vary widely, from the micrometer to the nanoscale.

4. Single Crystal X-ray Diffraction

Single crystal diffraction (SXRD) data was collected on XtaLAB SuperNova (Tianjin Key Laboratory of Molecular Optoelectronic Sciences) with Mo Kα radiation (40 kV, 50 mA). A suitable crystal was selected and the crystal was mounted on a magnetic holder with vacuum grease on diffractometer. The crystal was kept at 298 K during the data collection. Using Olex 2 [1], the structure was solved with the ShelXT structure solution program using Intrinsic Phasing and refined with the XL refinement package using Least Squares minimization [2].

Table S1. Crystal data and structure refinement for OFN-DMA.

CCDC Deposition Number	2211859
Empirical formula	$C_{26}H_{14}F_8$
Formula mass	478.37
Temperature / K	298.15
Crystal system	Triclinic
Space group	P -1
a / Å, b / Å, c / Å	6.8480(4), 8.8391(6), 9.0199(7)
α/°, β/°, γ/°	100.682(6), 102.679(6), 104.957(6)
Volume / Å^3	497.36(7)
Z	14
ρcalc / mg mm^{-3}	1.497
μ / mm^{-1}	0.179
F (000)	224.0
Crystal size / mm^3	0.15 × 0.1 × 0.05
2Θ range for data collection	6.418° to 58.968°
Index ranges	$-9 \leq h \leq 9$, $-11 \leq k \leq 11$, $-10 \leq l \leq 12$
Reflections collected	5521
Independent reflections	2370 [Rint = 0.0157]
Data/restraints/parameters	2370/0/155
Goodness-of-fit on F^2	1.050
Final R indexes [I>2σ (I)]	$R_1 = 0.0709$, $wR_2 = 0.1917$
Final R indexes [all data]	$R_1 = 0.0883$, $wR_2 = 0.2153$
Largest diff. peak/hole / e Å^{-3}	0.37/-0.48

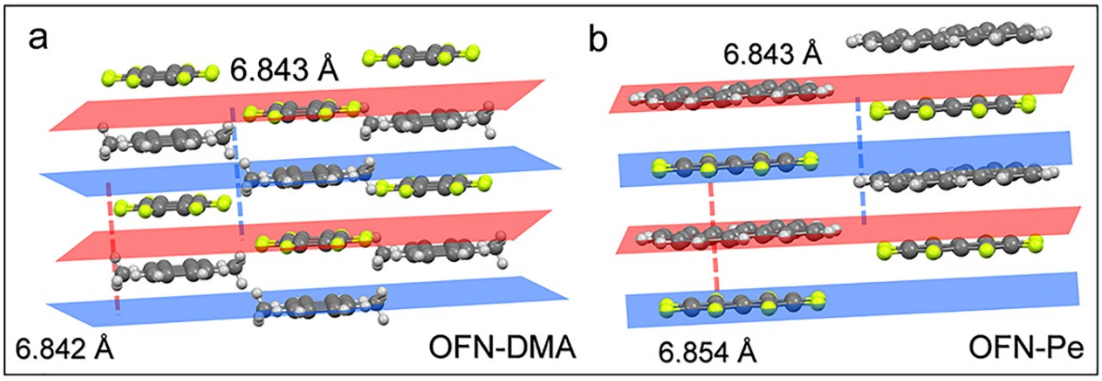

Fig. S3. Distance between donor and acceptor molecules. (a) OFN-DMA, and (b) OFN-Pe.

The following formula was used to calculate the distance:[3]

$$l = \frac{L_D + L_A}{4}$$

where l means the distance between the donor and the acceptor, L_D and L_A represent the distance between two donor molecules and two acceptor molecules, respectively.

As for OFN-DMA, the distance between donor and acceptor is $\frac{6.843 + 6.842}{4} = 3.42$ Å

As for OFN-Pe, the distance between donor and acceptor is $\frac{6.843 + 6.854}{4} = 3.42$ Å

5. Powder X-ray Diffraction

Powder XRD (PXRD) was obtained on the Rigaku SmartLab diffractometer (Tianjin Key Laboratory of Molecular Optoelectronic Sciences) made in Japan. Testing parameters: Cu Kα radiation, $\lambda = 1.5418$ Å, the power was set to 9 kW, the voltage was 45 kV, and the current was 200 mA. The single component molecules (OFN and DMA) for PXRD testing were purchased directly from the reagent company, properly ground and without any purification process.

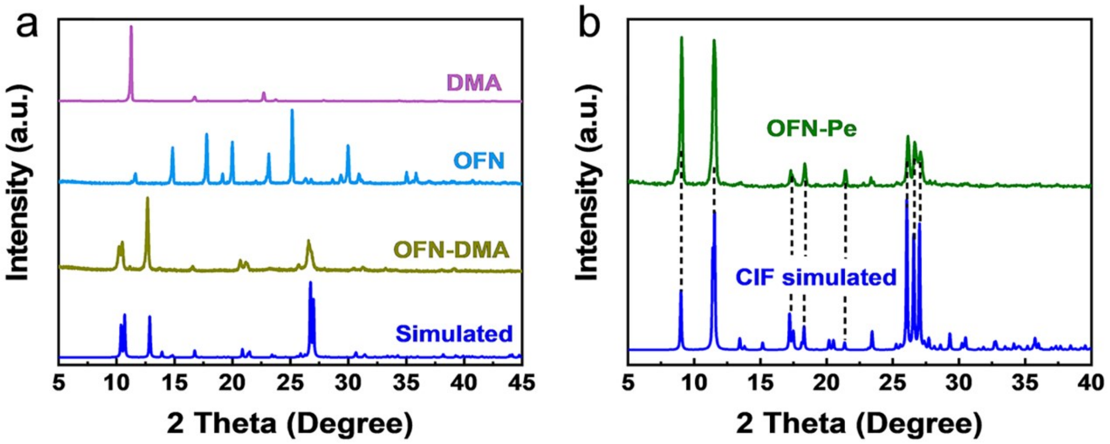

Fig. S4. Powder XRD pattern of cocrystals. (a) The PXRD results of DMA, OFN, and OFN-DMA, and calculated XRD pattern from the CIF file. (b) The PXRD results of OFN-Pe, and calculated XRD pattern from the CIF file.

6. FTIR Spectroscopy

Fourier transform infrared (FTIR) spectra was measured on a Vertex 70 (Bruker, Germany) spectrometer (Tianjin Key Laboratory of Molecular Optoelectronic Sciences). Before measurements, the solid powder was placed in oven at 60°C for 3 hours to dry and remove any water that may be contained on the materials. Nondestructive measurements were performed directly on powder samples using attenuated total reflection (ATR) mode, with diamond as the ATR crystal substrate. The detector was a photoconductive type mercury cadmium telluride (MCT) detector, adding the appropriate liquid nitrogen to reduce the noise signal. The single component molecules for FTIR measurements were purchased directly from the reagent company, properly ground and without any purification process. Cocrystal powder was directly obtained by liquid-assisted grinding for testing.

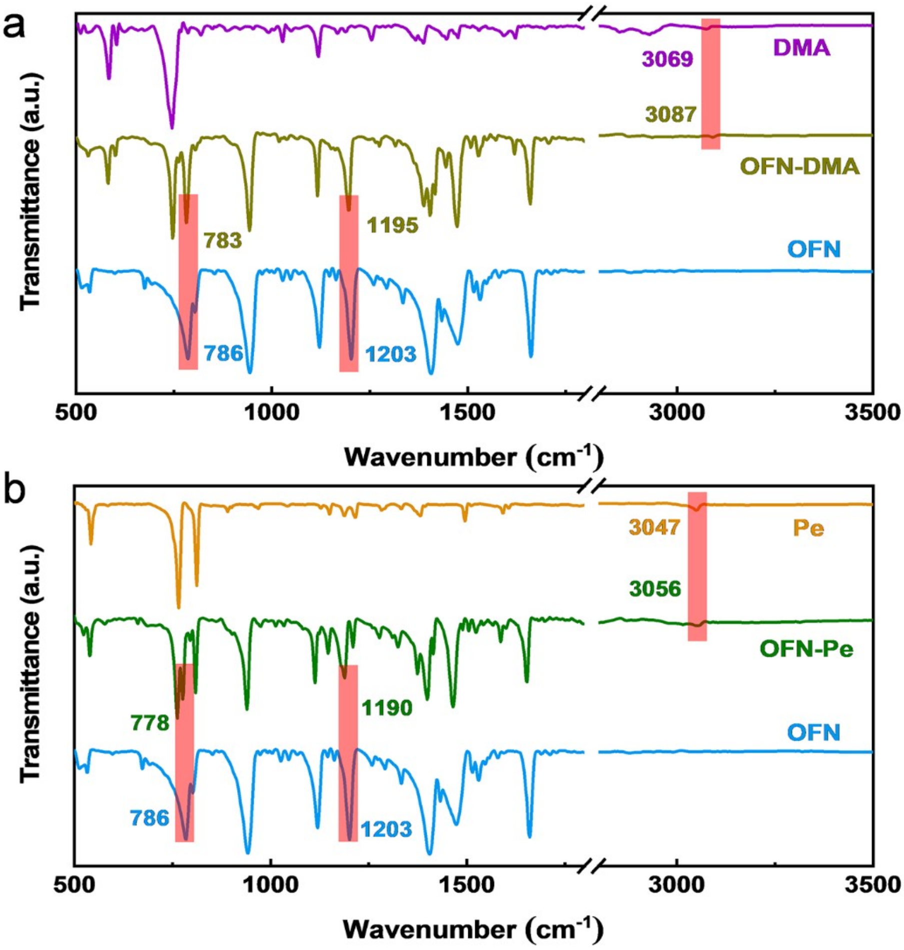

Fig. S5. FTIR spectrum of cocrystal and monomer. (a) OFN, DMA, and OFN-DMA. (b) OFN, Pe, and OFN-Pe.

7. UV-Vis Absorption and Photoluminescence Spectroscopy

The UV-3600 Plus (SHZMADZU, Japan) spectrophotometer (Tianjin Key Laboratory of Molecular Optoelectronic Sciences) combined with diffuse reflectance mode integrating sphere was used for testing the UV-visible diffuse reflectance spectrum. A small amount of the powder under test was evenly applied to the $BaSO_4$ substrate. A baseline test of the blank $BaSO_4$ was required to eliminate substrate effects before testing the sample. Wherein, the single component molecules for UV absorption measurements were purchased directly from the reagent company, properly ground and without any purification process. Cocrystal powder was directly obtained by liquid-assisted grinding for testing.

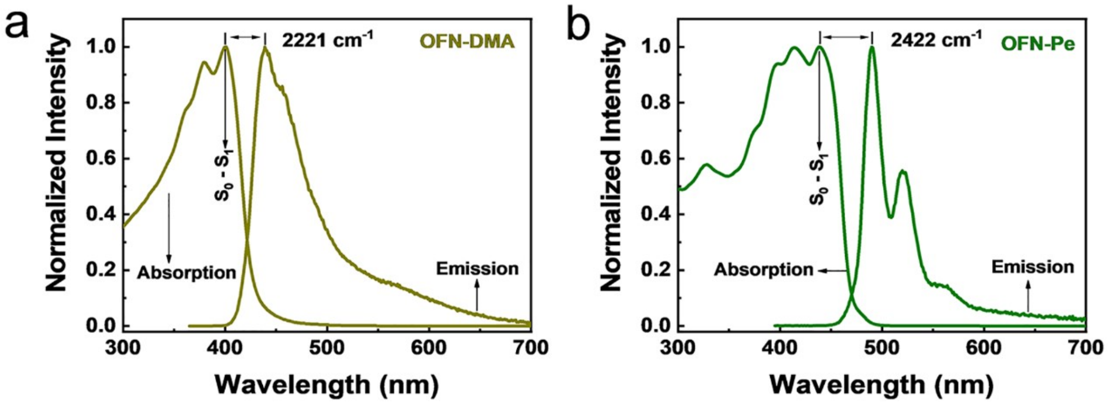

Fig. S6. Stokes shift values of cocrystal. (a) OFN-DMA, and (b) OFN-Pe.

The Stokes shift values for OFN-DMA and OFN-Pe are 2221 cm^{-1} and 2422 cm^{-1}, respectively. The smaller values (< 3000 cm^{-1}) imply a lower change in the molecular configuration at ground state [4], confirm the absence of charge transfer (CT) interactions, and indirectly corroborate the AP interactions in the cocrystals.

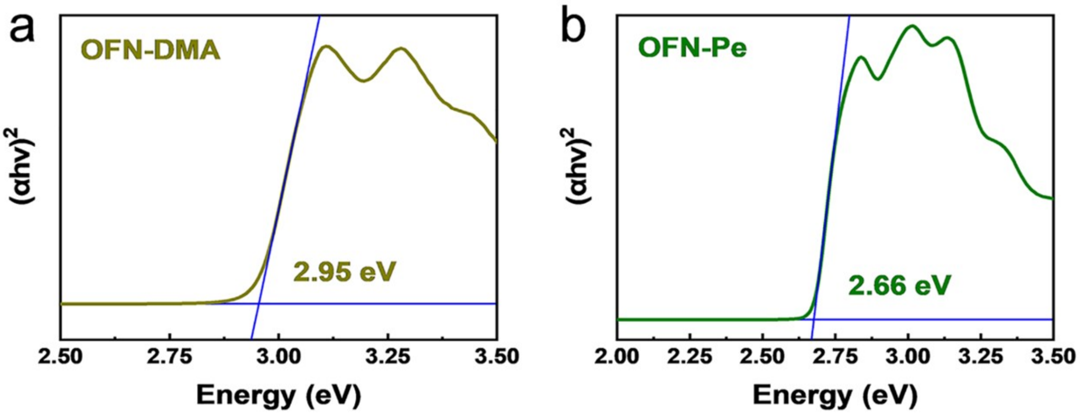

Fig. S7. Tauc plots for the band gap energy. (a) OFN-DMA, and (b) OFN-Pe.

8. Photocatalytic Measurements

General experiment: Photocatalytic material (50 mg) was dispersed in pollutant solution (50 mL, 30 ppm) and sonicated for 10 min to form a homogeneous suspension. Then, photocatalytic measurement was started after dark treatment for 30 min [5]. 2 mL samples were collected at specific time intervals, the sample solution was purified by 0.22 μm microporous filtration membrane to remove the solid catalyst. Finally, the clarified liquid was measured on a UV spectrophotometer for concentration determination. A 300 W Xe lamp (Perfect Light, PLS-SXE300D/300DUV) with a 400 nm filter served as the simulated light source. Optical power meter (China Education Au-light, CEL-NP2000-10A) was used to test the light intensity during the experiment.

Calculation of catalytic efficiency: The rate of pollutant degradation was fitted with the quasi-first kinetic equation $-\ln (C_t/C_0) = k_{ap}$ [6]. Where, C_0 and C_t represent the initial pollutant concentration and the concentration after t minutes of light irradiation, t represents the reaction time, and k_{ap} is the rate constant of the degradation reaction.

Synthesis of g-C_3N_4: The most commonly used pristine g-C_3N_4 in literatures was synthesized through the thermal polymerization method [7]. Namely, melamine was calcined at 550 °C for 2 h with a heating rate of 5 °C min^{-1} under air atmosphere. The obtained yellow-colored powder was denoted as g-C_3N_4 (Carbon Nitride).

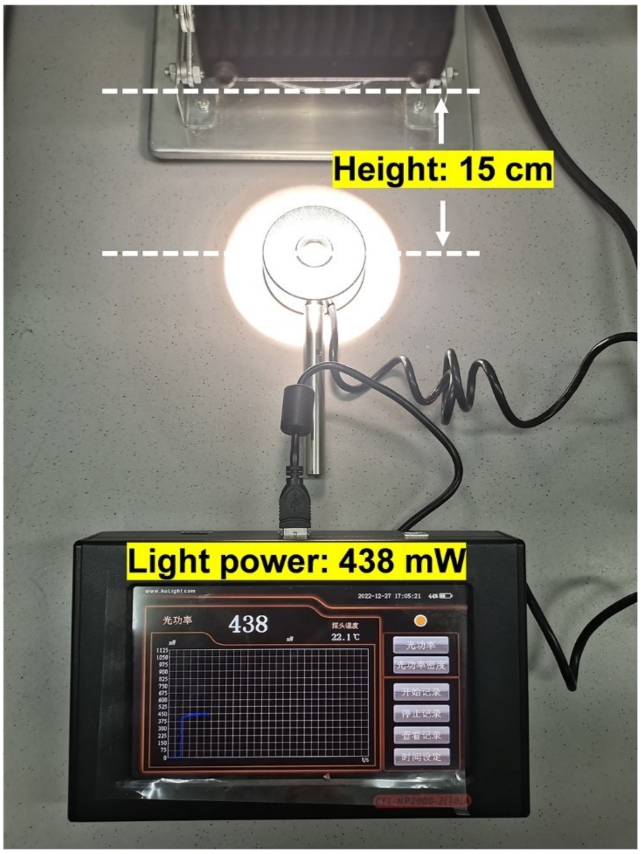

Fig. S8. Power of Xe lamp used for the photocatalytic experiments.

8.1. Effects of Catalyst Concentration

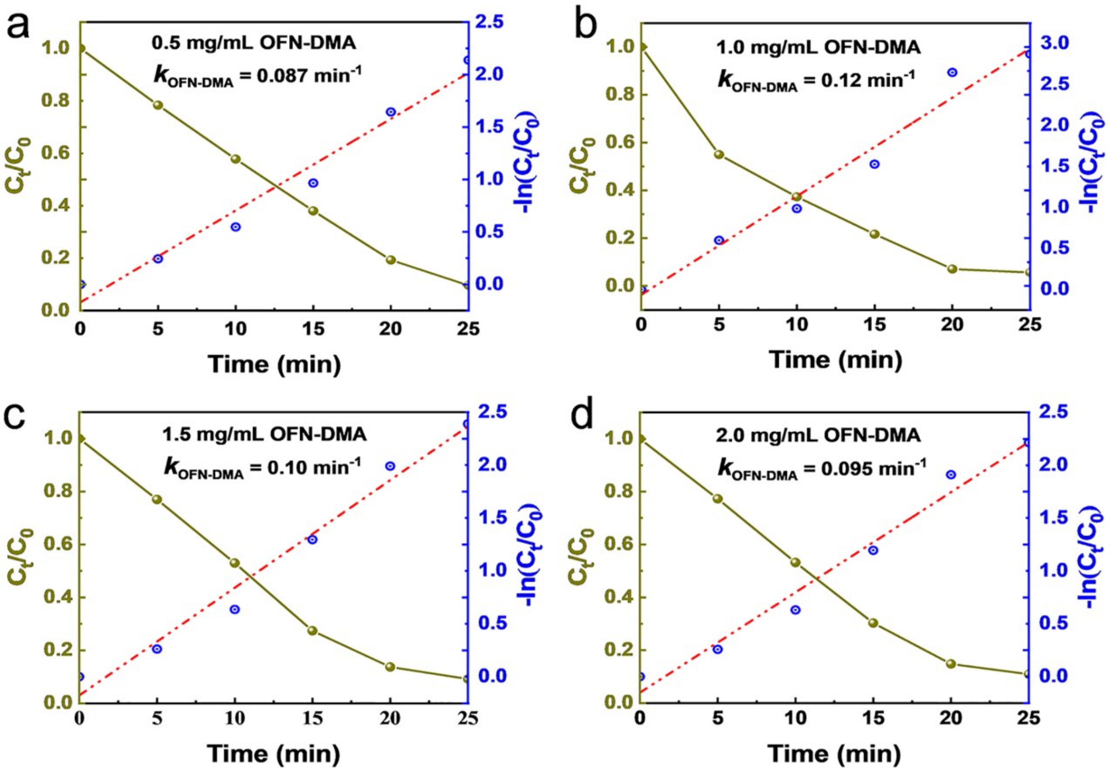

Fig. S9. The effect of different OFN-DMA concentrations on catalytic performance. The concentrations of OFN-DMA are set to (a) 0.5 mg mL^{-1}, (b) 1 mg mL^{-1}, (c) 1.5 mg mL^{-1}, and (d) 2.0 mg mL^{-1}, respectively.

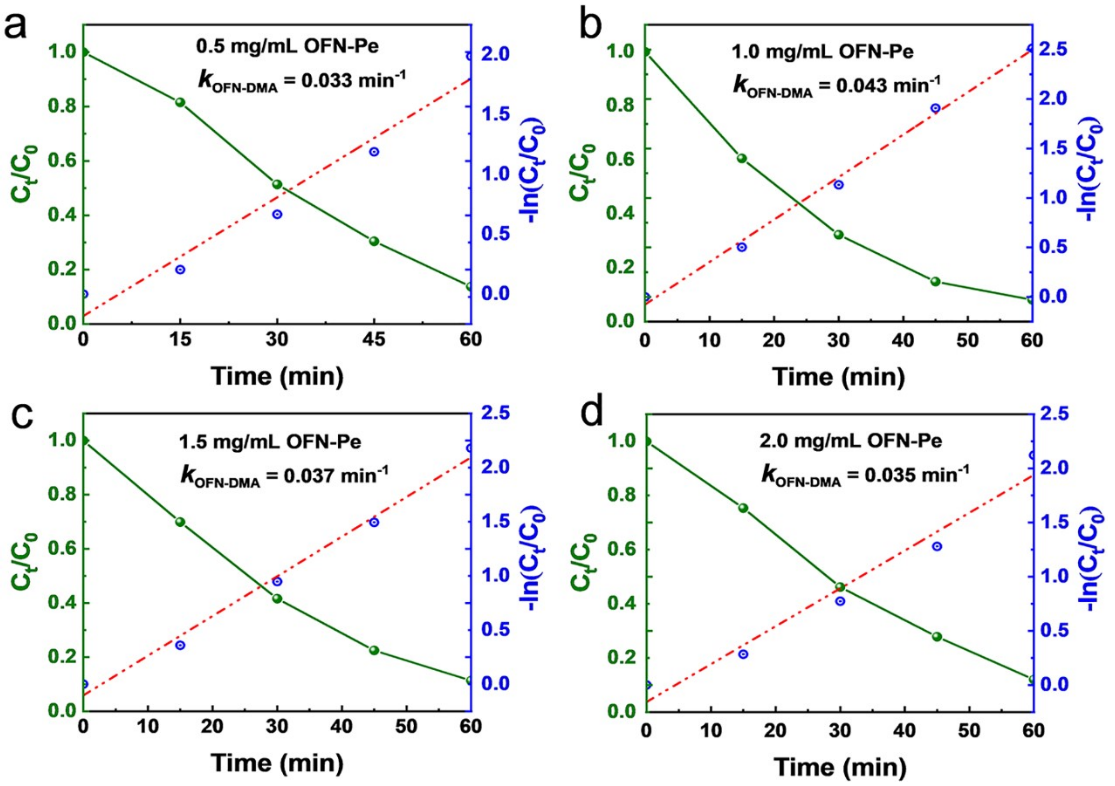

Fig. S10. The effect of different OFN-Pe concentrations on catalytic performance. The concentrations of OFN-Pe are set to (a) 0.5 mg mL^{-1}, (b) 1 mg mL^{-1}, (c) 1.5 mg mL^{-1}, and (d) 2.0 mg mL^{-1}, respectively.

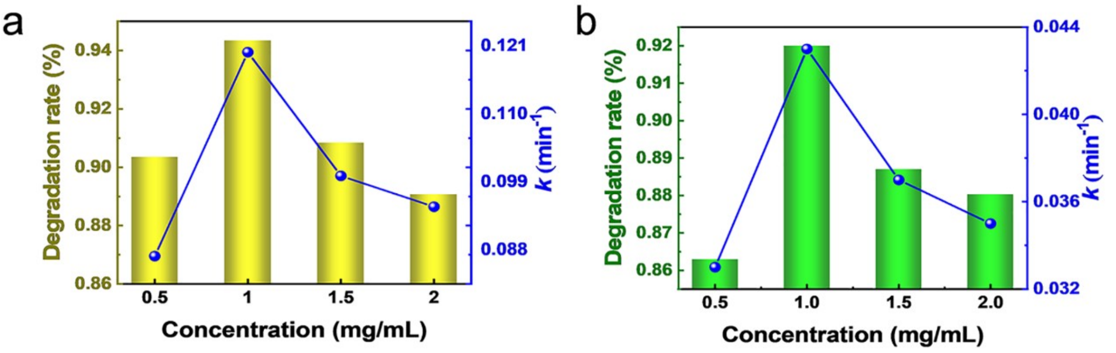

Fig. S11. Relationship between different concentrations and catalytic performance. (a) OFN-DMA. (b) OFN-Pe.

As shown in Fig. S11, the catalyst concentration of 1 mg mL^{-1} is most favorable for the photocatalytic reaction. High concentrations of pollutants cannot be adequately degraded by smaller amounts of catalyst (0.5 mg mL^{-1}), causing a slower reaction rate [8]. When large amounts of catalyst are added (>1 mg mL^{-1}), the light transmission of water is weakened because of the presence of too abundant solids [9].

8.2. Brunauer Emmett Teller (BET) measurements and Specific Activity

Micromeritics TriStar 3000 (United States of America) physisorption instrument was used to test the specific surface area of catalysts. The specific surface area curves were determined by nitrogen low temperature adsorption method in the specific surface area mode. The samples were evacuated and degassed at 120 °C for 8 hours to remove the impurity gases adsorbed on the surface, and then the adsorption and desorption measurement procedures were performed at liquid nitrogen temperature.

Table S2. The specific activity per unit area of P25, g-C_3N_4, and OFN-Pe.

	P25	g-C_3N_4	OFN-Pe
k [min^{-1}]	0.058	0.046	0.044
BET Surface [$m^2\ g^{-1}$]	90.0936	5.1379	0.4037
Mass [mg]	50	50	50
Surface [m^2]	4.5047	0.2569	0.02019
K [$\text{min}^{-1}\ m^{-2}$]	0.013	0.18	2.18

Catalytic efficiency is greatly influenced by the specific surface area of the catalyst, and high specific surface area usually provide more reactive sites to accelerate the photocatalytic reaction. The catalytic effect of different materials is more distinctly reflected by the specific activity per unit area. According to relevant report [10], the specific activity per unit area can be expressed by the following formula:

$$K = \frac{k}{m \times A}$$

where K ($\text{min}^{-1}\ m^{-2}$) is the specific activity per unit area, k (min^{-1}) is the reaction rate constant, m (g) is the actual mass engaged in the photocatalytic reaction, and A ($m^2\ g^{-1}$) is the Brunauer Emmett Teller (BET) specific surface area of the photocatalytic material.

8.3. Cyclic Stability

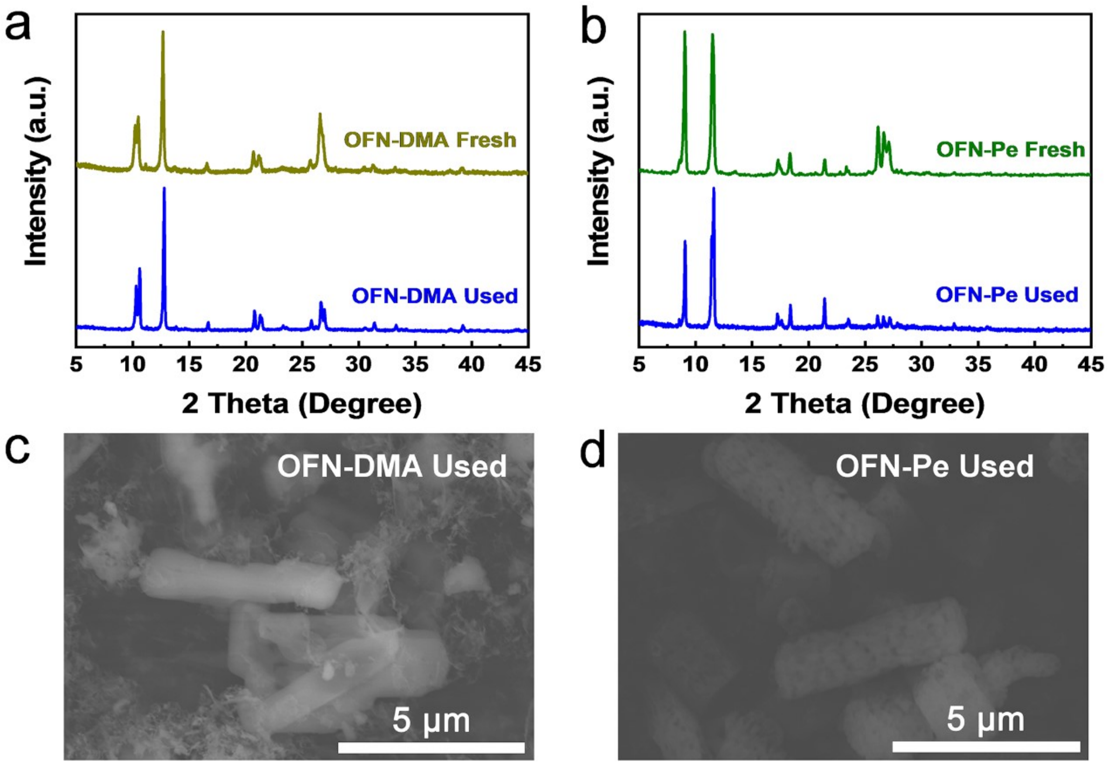

Fig. S12. PXRD and SEM of cocrystals before and after using as photocatalyst for pollutant degradation.

8.4. Universal Analysis of Photocatalysis

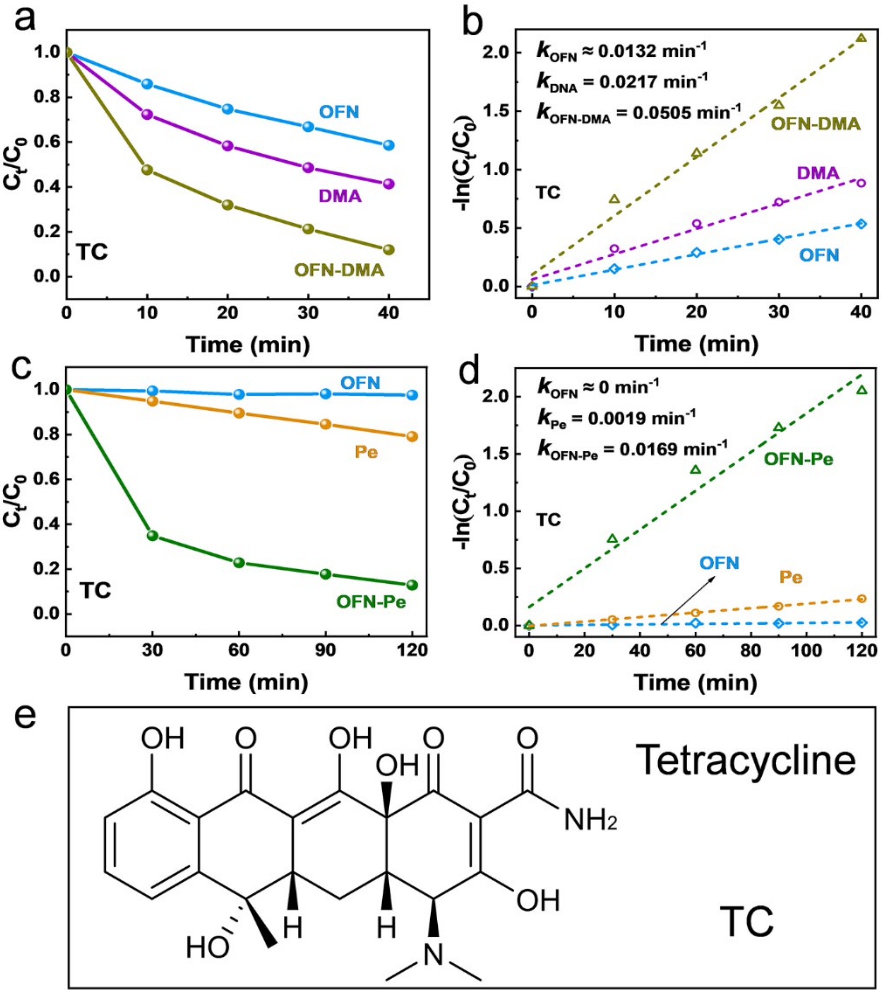

Fig. S13. The photocatalytic degradation performance of TC. (a) Degradation curves of OFN, DMA, OFN-DMA with time under 300~780 nm light irradiation. (b) Quasi-first kinetic curves fitting for OFN-DMA cocrystal photocatalytic degradation of TC. (c) Degradation curves of OFN, Pe, OFN-Pe with time under 400~780 nm light irradiation. (d) Quasi-first kinetic curves fitting for OFN-Pe cocrystal photocatalytic degradation of TC. (e) Chemical structure formula of tetracycline.

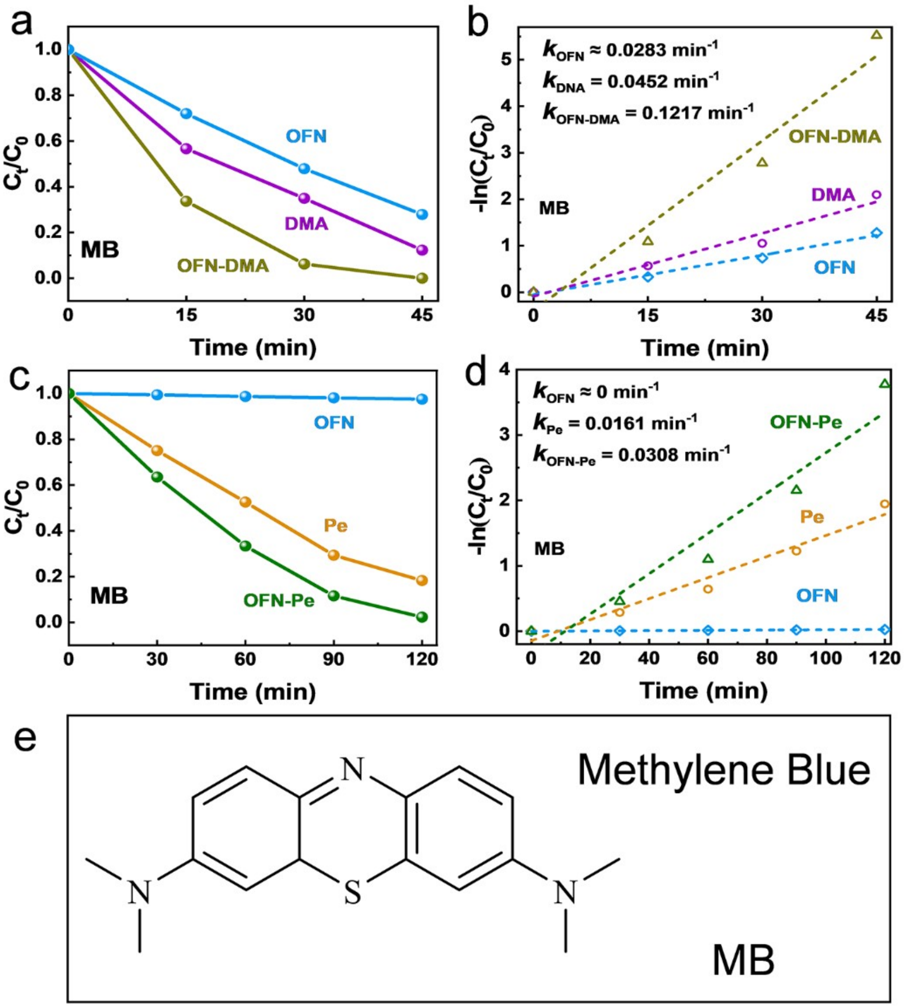

Fig. S14. The photocatalytic degradation performance of MB. (a) Degradation curves of OFN, DMA, OFN-DMA with time under 300~80 nm light irradiation. (b) Quasi-first kinetic curves fitting for OFN-DMA cocrystal photocatalytic degradation of MB. (c) Degradation curves of OFN, Pe, OFN-Pe with time under 400~780 nm light irradiation. (d) Quasi-first kinetic curves fitting for OFN-Pe cocrystal photocatalytic degradation of MB. (e) Chemical structure formula of methylene blue.

For the degradation of TC, the degradation rate of OFN-DMA is 3.83 and 2.33 times higher than OFN, DMA, respectively. The degradation rate of OFN-Pe is 8.89 times higher than Pe. As for the degradation of MB, the degradation rate of OFN-DMA is 4.30 and 2.69 times compared to OFN, DMA. The degradation rate of OFN-Pe is 1.91 times higher than Pe.

Table S3. Comparison of pollutant degradation performance of different organic catalysts.

Catalyst	Pollutant	Light	Pollutant Concentration [ppm]	Degradation time [min]	k [min^{-1}]	Refs.
Zinc phthalocyanine	RhB	150 W Xe lamp ($\lambda > 400$ nm)	10	690	/	11
PDI-NH	RhB	300 W Xe lamp ($\lambda > 420$ nm)	~15	480	~0.0022	12
PDI-CH_3	RhB	5 W LED lamp	10	210	0.0028	13
PDI-NH_2	RhB	5 W LED lamp	10	210	0.0035	13
PDI-COOH	RhB	5 W LED lamp	10	210	0.0092	13
Polypyrrole	RhB	300 W Xe lamp (Full spectrum)	20	360	/	14
OFN-Pe	RhB	300 W Xe lamp ($400 < \lambda < 780$ nm)	30	60	0.044	This work
OFN-DMA	RhB	300 W Xe lamp ($300 < \lambda < 780$ nm)	30	25	0.12	This work
SA-PDI	TC	300 W Xe lamp ($\lambda > 400$ nm)	20	/	~0.006	15
3D-PDI	TC	5 W LED lamp ($\lambda > 420$ nm)	20	150	0.0074	16
PDI-CH_3	TC	5 W LED lamp	20	120	0.0048	13
PDI-NH_2	TC	5 W LED lamp	20	120	0.0062	13
PDI-COOH	TC	5 W LED lamp	20	120	0.012	13
OFN-Pe	TC	300 W Xe lamp ($400 < \lambda < 780$ nm)	30	120	0.0169	This work
OFN-DMA	TC	300 W Xe lamp ($300 < \lambda < 780$ nm)	30	40	0.0505	This work
ANP	MB	300 W Xe lamp ($\lambda > 420$ nm)	~30	200	/	17
PDI-NH	MB	300 W Xe lamp ($\lambda > 420$ nm)	~10	480	~0.0060	12

Table S3 Continued.

Catalyst	Pollutant	Light	Pollutant Concentration [ppm]	Degradation time [min]	k [min^{-1}]	Refs.
PDI-CH_3	MB	5 W LED lamp	20	150	0.0043	13
PDI-NH_2	MB	5 W LED lamp	20	150	0.0077	13
PDI-COOH	MB	5 W LED lamp	20	150	0.021	13
Tetraphenyl-porphyrin	MB	500 W Xe lamp ($\lambda > 400$ nm)	~3	240	/	18
Polypyrrole	MB	300 W Xe lamp (Full spectrum)	20	360	/	14
OFN-Pe	MB	300 W Xe lamp ($400 < \lambda < 780$ nm)	30	120	0.0308	This work
OFN-DMA	MB	300 W Xe lamp ($300 < \lambda < 780$ nm)	30	45	0.1217	This work

9. Ultraviolet Photoelectron Spectroscopy (UPS)

Ultraviolet photoelectron spectroscopy (UPS) measurements were carried out on a Thermo Scientific Escalab 250Xi spectrometer (Analysis and Testing Center, Tianjin University). He I was used as the excitation source with an energy of 21.22 eV. Gold specimens (Fermi edge at 0.0 eV) were used to calibrate the instrument.

The highest occupied orbit (HOMO) is calculated from the following equation:[19]

$$-\mathrm{HOMO} = h\nu - (E_{cutoff} - E_{onset})$$

where $h\nu$ is the photoenergy of He I source (21.22 eV), E_{onset} is binding energy onset, E_{cutoff} is binding-energy cutoffs.

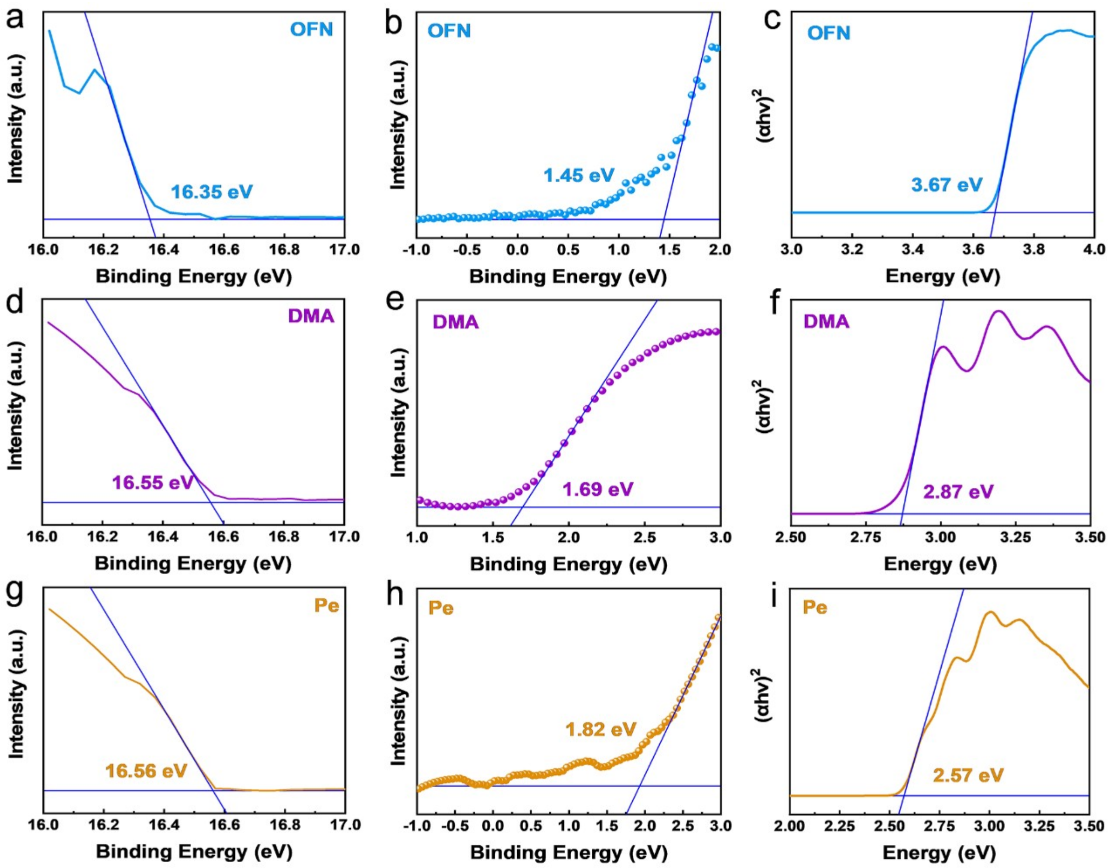

Fig. S15. UPS energy spectra of monomeric molecules. (a) Secondary electrocutoff of OFN. (b) HOMO band of OFN. (c) Tauc plots for the band gap energy of OFN. (d) Secondary electrocutoff of DMA. (e) HOMO band of DMA. (f) Tauc plots for the band gap energy of DMA. (g) Secondary electrocutoff of Pe. (h) HOMO band of Pe. (i) Tauc plots for the band gap energy of Pe.

Table S4. Summary HOMO, LUMO and bandgap, calculated from UPS spectra and UV-vis spectra.

	Cutoff tail [eV]	Fermi tail [eV]	E_g [eV]	HOMO [eV]	LUMO [eV]
OFN	16.35	1.45	3.67	-6.32	-2.65
DMA	16.55	1.69	2.87	-6.36	-3.49
Pe	16.56	1.82	2.57	-6.48	-3.91
OFN-DMA	16.22	0.88	2.95	-5.88	-2.93
OFN-Pe	16.18	0.58	2.66	-5.62	-2.96

10. Radical Quenching Experiments

The types of radicals generated during photocatalysis were demonstrated initially by radical quenching experiments. Ascorbic acid (AA), isopropyl alcohol (IPA), and ethylenediamine (TEA) were used as quenchers of $\cdot O_2^-$, $\cdot OH$ and h^+, respectively [20]. According to the published report, the quencher concentration should be 10 mM [21].

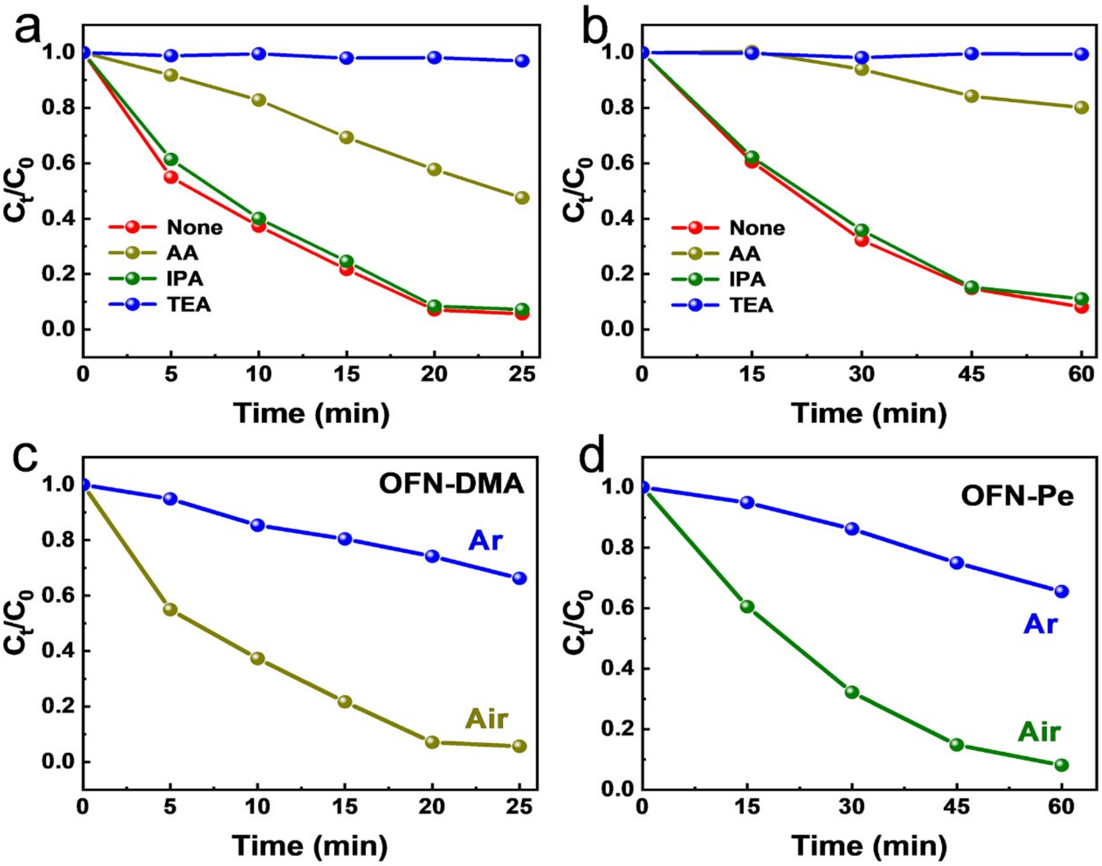

Fig. S16. Photocatalytic degradation of RhB under different conditions. Active radical quenching experiments of (a) OFN-DMA, and (b) OFN-Pe. Degradation curves under different gas conditions of (c) OFN-DMA, and (d) OFN-Pe.

11. Electron Paramagnetic Resonance (EPR) Spectroscopy

Electron paramagnetic resonance spectrometer (EPR, Bruker EMXplus) was used to detect the active species produced during the catalytic process. The test procedure as follows: 500 μL of catalyst sample (2 mg mL^{-1}) was added to 500 μL of 5,5-dimethyl-1-pyrroline N-oxide (DMPO) solution (100 mM) and sonicated to disperse the sample uniformly. The signal was then tested after irradiation with a Xe lamp. DMPO methanol solution was used to detect superoxide radicals ($\cdot O_2^-$) and DMPO aqueous solution was used to detect hydroxyl radicals (·OH) [22]. A free radical curve (dark) was obtained by measurement without light irradiation treatment. Then another free radical curve (light) was obtained after 10 minutes continuous illumination using [23]. The light source conditions (300 W Xe lamp) were kept identical to the photocatalytic experiment.

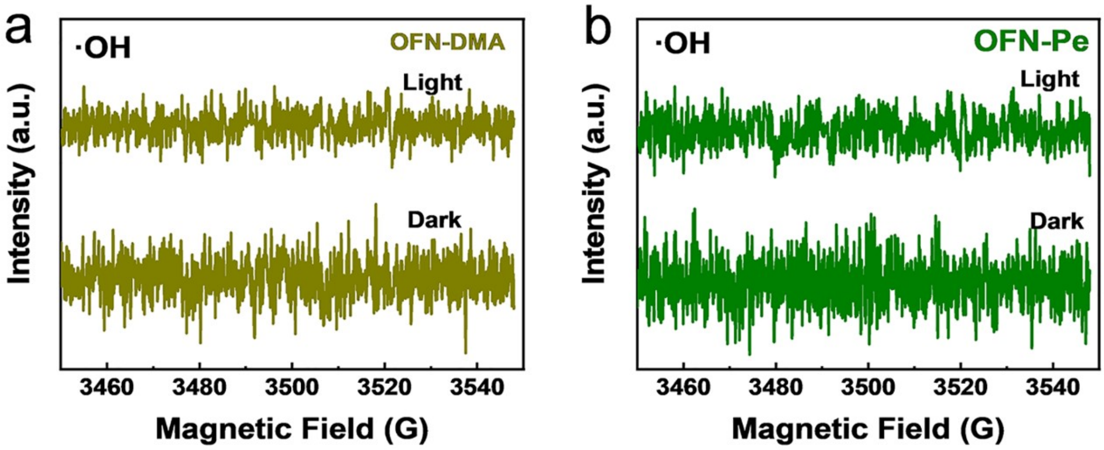

Fig. S17. EPR spectra for the detection of ·OH. (a) OFN-DMA, and (b) OFN-Pe.

12. Atomic Force Microscopy (AFM)

Kelvin Probe Force Microscopy (KPFM) is an electrostatic force microscopy technique applied to test the electrical potential distribution on the sample surface, it has been widely applied to heterojunction materials, donor-acceptor (D-A) organic photocatalysts to determine the strength of the IEF. Briefly, a bias pressure is applied between the cantilever probe and the sample, and then a surface potential distribution map is created from the potential difference between the sample and the probe tip.

KPFM was performed on a Bruker Dimension Icon microscope (Tianjin Key Laboratory of Molecular Optoelectronic Sciences) under ambient atmosphere in the amplitude-modulated (AM-KPFM) mode. The test procedure as follows: THF solutions of OFN, DMA, Pe, OFN-DMA, and OFN-Pe (0.25 mg mL^{-1}) were dropped on bare Si substrate to obtain micro-nano crystals. Vacuum drying at 60°C for about 2 hours was performed to remove residual solvent for measurements. The Si substrate with the sample was fixed on the sample stage using conductive glue to keep the crystal and the sample stage in conduction during the measurement. During the measurement of surface potential, the lift mode was used with a lift height of 50 nm. The obtained data were processed using NanoScope Analysis software to obtain surface potential images and the corresponding contact potential difference profiles.

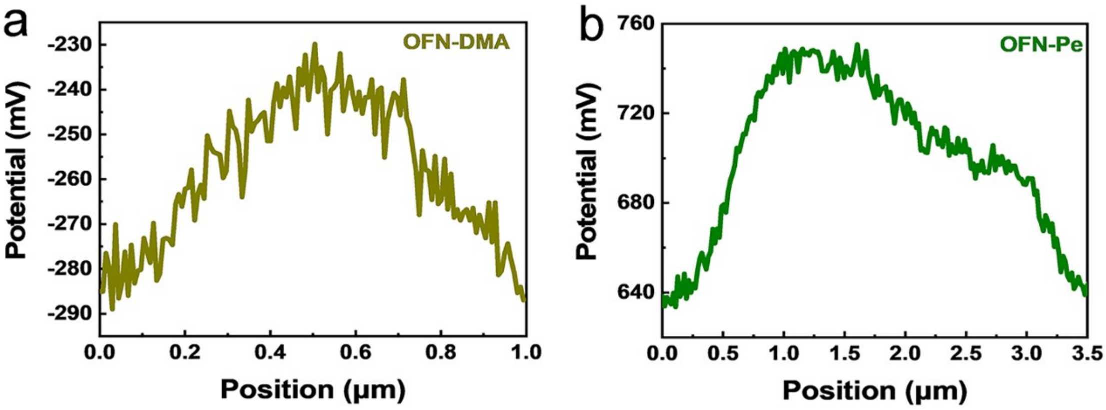

Fig. S18. Contact potential difference profiles of cocrystals. (a) OFN-DMA micro-nano cocrystal, and (b) OFN-Pe micro-nano cocrystal.

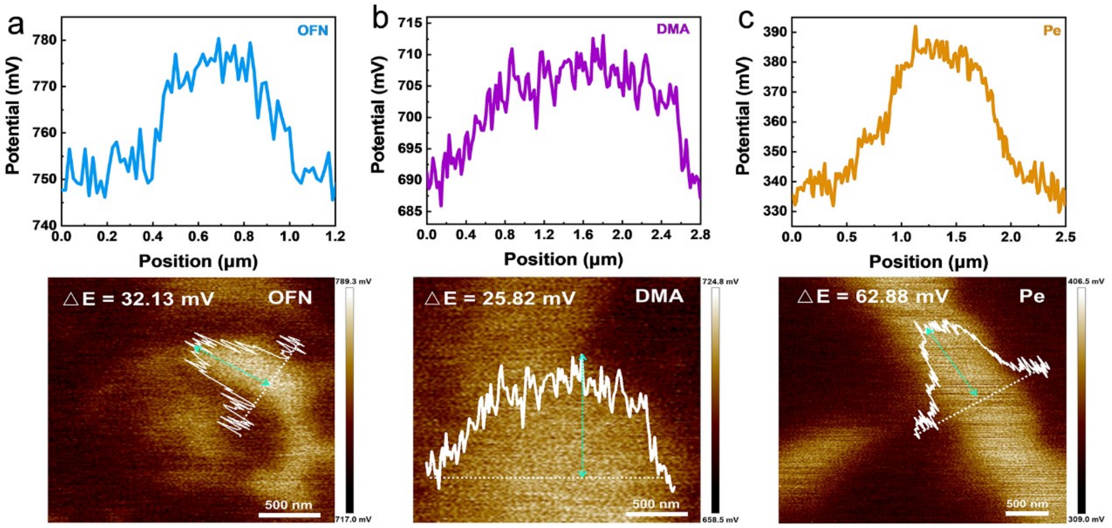

Fig. S19. Contact potential difference profiles of cocrystals. (a) OFN-DMA micro-nano cocrystal, and (b) OFN-Pe micro-nano cocrystal.

13. Photoluminescence Microscopy and Time-resolved fluorescence spectroscopy

Time-resolved fluorescence spectroscopy and fluorescence decay lifetime were measured on an Edinburgh FLS1000 fluorescence spectrometer (Institute of Molecular Aggregation Science, Tianjin University). Emission spectroscopy was detected using a gated spectral scan mode with a 450 W Xe lamp (pulse width <2 μs) as the excitation source. nF920 nanosecond lamp and an EPL-375 3B laser were used for fluorescence lifetime measurements. Wherein, the single component molecules for testing were purchased directly from the reagent company, properly ground and without any purification process. Cocrystal powder was directly obtained by liquid-assisted grinding for testing. The monitored wavelengths of DMA, OFN-DMA, Pe, and OFN-Pe are 520 nm, 450 nm, 590 nm, and 490 nm, respectively.

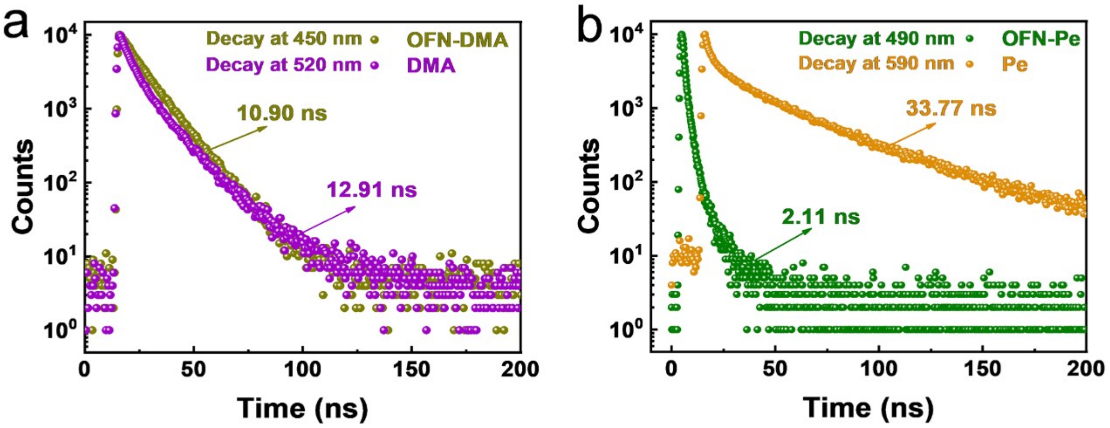

Fig. S20. Contact potential difference profiles of cocrystals. (a) OFN-DMA micro-nano cocrystal, and (b) OFN-Pe micro-nano cocrystal.

Table S5. Fluorescence decay lifetime of monocrystals and cocrystals.

	DMA	Pe	OFN-DMA	OFAN-Pe
$\tau1$ [ns]	6.1359	2.5483	6.9288	1.1624
Rel.%	33.70	9.32	37.79	69.56
$\tau2$ [ns]	15.4910	19.3395	12.2432	3.2017
Rel.%	63.41	38.22	62.21	27.10
$\tau3$ [ns]	35.0000	49.8309	\	13.1527
Rel.%	2.89	52.45	\	3.34
τ [ns]	12.90	33.77	10.23	2.11
χ^2	1.0662	1.2096	1.2588	1.2056

14. Electrochemical Impedance Spectroscopy (EIS)

The photoelectrochemical properties of the cocrystal catalysts were measured in electrochemical workstations (CHI760E, Tianjin Key Laboratory of Molecular Optoelectronic Sciences) manufactured by Shanghai Chenhua company. Electrochemical impedance spectroscopy (EIS) was carried out in the three-electrode system. The modified glassy carbon electrode, platinum sheet electrode and Ag/AgCl electrode were used as the working electrode, counter electrode, and reference electrode, respectively. A 300 W Xe lamp was used as excitation light source, Na_2SO_4 solution (0.5 M) was used as electrolyte. The EIS were collected with the frequency range between 1×10^6 Hz to 1 Hz.

Preparation conditions for working electrodes: the sample was sonicated and dispersed into water form a homogeneous suspension at a concentration of 2 mg mL^{-1}. The suspension (20 μL) was added dropwise to working electrode and dried at room temperature for 12 h, and then working electrode was dried at 60°C for about 3 hours.

Electrochemical Impedance Spectroscopy data was processed by using ZSimpWin software. Model R(Q(RW)) was chosen to fit the data to obtain the corresponding impedance values [24].

Table S6. Charge transfer resistance of monomers and cocrystals.

	R_L [Ω]	R_{CT} [Ω]
OFN	49.11	1461.0
DMA	51.14	972.2
Pe	51.79	617.8
OFN-DMA	49.62	475.6
OFN-Pe	53.80	348.8

15. Computation of Intermolecular Electronic Couplings

The electronic couplings for intermolecular electron and hole transfer between two molecules were computed using the method of configuration interaction based on constrained density functional theory (CDFT-CI) [25, 26]. All the calculations were performed at the B3LYP/6-311++G** level using the Q-chem 6.0 package [27-29]. Solvent effect was included with the CPCM model, and the dielectric constant of the anthracene solvent was utilized [30, 31].

The crystal structure of OFN-DMA (CCDC No. 2211859) was obtained by our experimental determination. The crystal structures of OFN (CCDC No. 177726) [32], DMA (CCDC No. 1142508) [33], Pe (CCDC No. 1231185) [34], and OFN-Pe cocrystal (CCDC No. 1867077) [35] were obtained directly from The Cambridge Crystallographic Data Centre. The results of relatively large electronic couplings are summarized in the following Tables.

Table S7. The calculated electron and hole transfer couplings of the molecular dimers from the monocrystal of OFN.

		V_{ET} [cm^{-1}]	V_{HT} [cm^{-1}]
OFN monocrystal	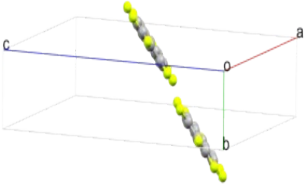	2	9
	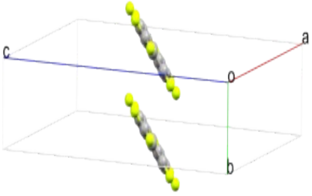	507	366
	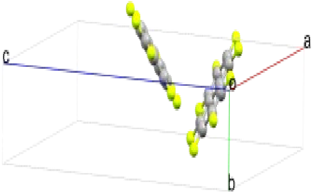	613	664

Table S8. The calculated electron and hole transfer couplings of the molecular dimers from the monocrystal of DMA.

		V_{ET} [cm^{-1}]	V_{HT} [cm^{-1}]
DMA monocrystal	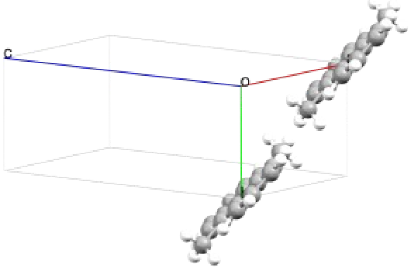	152	118
	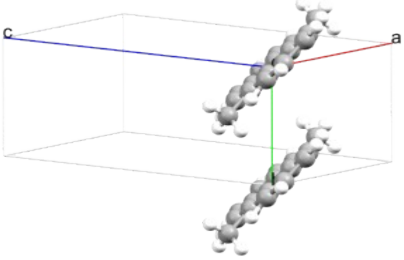	741	82
	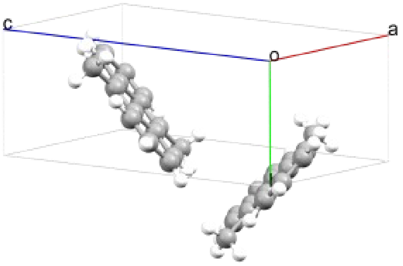	456	564

Table S9. The calculated electron and hole transfer couplings of the molecular dimers from the monocrystal of Pe.

		V_{ET} [cm^{-1}]	V_{HT} [cm^{-1}]
Pe monocrystal	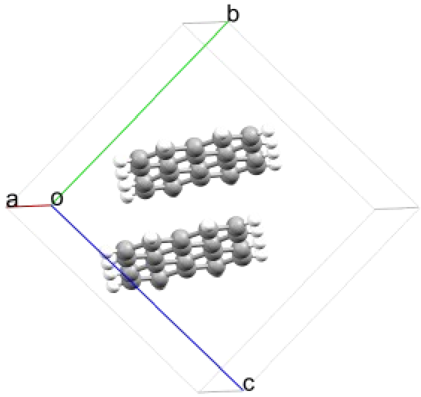	613	477
	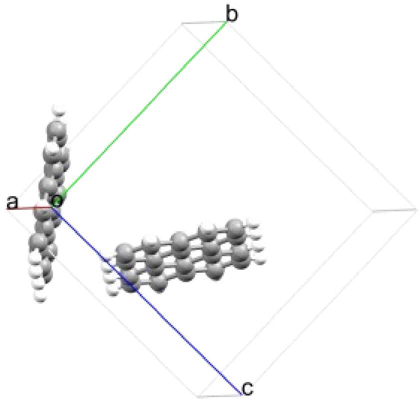	709	428
	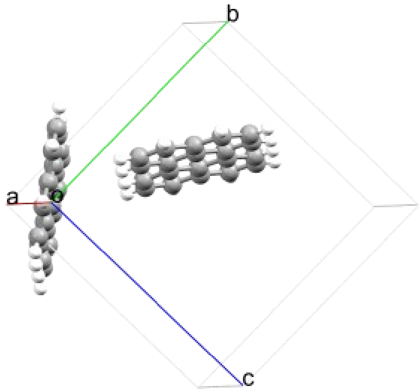	556	598

Table S10. The calculated electron and hole transfer couplings of the molecular dimers from the cocrystal of OFN-DMA.

		V_{ET} [cm^{-1}]	V_{HT} [cm^{-1}]
OFN-DMA cocrystal	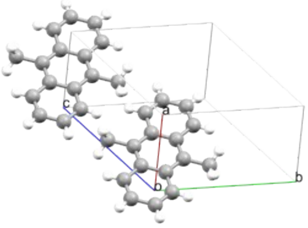	19	116
	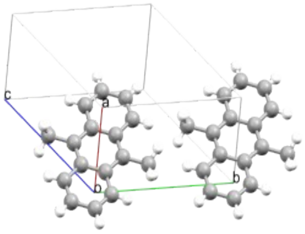	8	63
	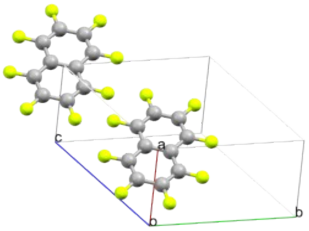	36	32
	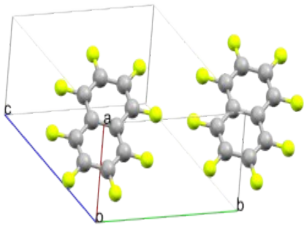	10	18

Table S11. The calculated electron and hole transfer couplings of the molecular dimers from the cocrystal of OFN-Pe.

		V_{ET} [cm^{-1}]	V_{HT} [cm^{-1}]
OFN-Pe cocrystal	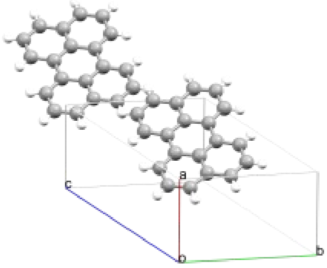	85	141
	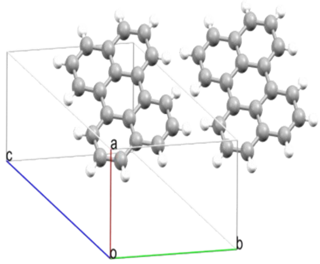	333	83
	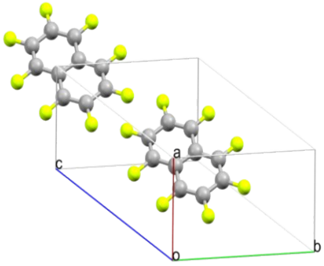	6	6
	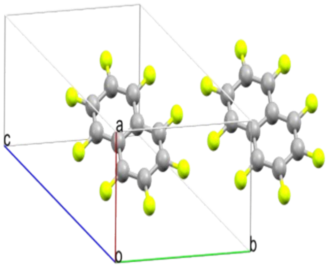	36	40

16. References

1. O. V. Dolomanov, L. J. Bourhis, R. J. Gildea, J. A. K. Howard and H. Puschmann, *J. Appl. Crystallogr.*, 2009, **42**, 339-341.
2. G. Sheldrick, *Acta Crystallogr. Sect. A: Found. Crystallogr.*, 2015, **71**, 3-8.
3. Y. Zhang, H. Wu, Y. Wang, L. Sun, S. Li, Y. Ren, Y. Sun, F. Yang, X. Zhang and W. Hu, *J. Mater. Chem. C*, 2022, **10**, 2562-2568.
4. W. Zhu, R. Zheng, X. Fu, H. Fu, Q. Shi, Y. Zhen, H. Dong and W. Hu, *Angew. Chem. Int. Ed.*, 2015, **54**, 6785-6789.
5. Z. Zhang, J. Wang, D. Liu, W. Luo, M. Zhang, W. Jiang and Y. Zhu, *ACS Appl. Mater. Interfaces*, 2016, **8**, 30225-30231.
6. Z. Yang, Y. Shi, H. Li, C. Mao, X. Wang, X. Liu, X. Liu and L. Zhang, *Environ. Sci. Technol.*, 2022, **56**, 3587-3595.
7. B. Zhai, H. Li, G. Gao, Y. Wang, P. Niu, S. Wang and L. Li, *Adv. Funct. Mater.*, 2022, **32**, 2207375.
8. Y. Hou, F. Liu, B. Zhang and M. Tong, *Environ. Sci. Technol.*, 2022, **56**, 16303-16314.
9. T. Cheng, H. Gao, R. Li, S. Wang, Z. Yi and H. Yang, *Appl. Surf. Sci.*, 2021, **566**, 150669.
10. J. Liu, S. Zhang and H. Zhao, *Appl. Surf. Sci.*, 2019, **479**, 247-252.
11. Z. Guo, B. Chen, M. Zhang, J. Mu, C. Shao and Y. Liu, *J. Colloid Interface Sci.*, 2010, **348**, 37-42.
12. D. Liu, J. Wang, X. Bai, R. Zong and Y. Zhu, *Adv. Mater.*, 2016, **28**, 7284-7290.
13. Y. Pu, F. Bao, D. Wang, X. Zhang, Z. Guo, X. Chen, Y. Wei, J. Wang and Q. Zhang, *Journal of Environmental Chemical Engineering*, 2022, **10**, 107123.
14. Y. Li, S. Yan, X. Jia, J. Wu, J. Yang, C. Zhao, S. Wang, H. Song and X. Yang, *Appl. Catal. B: Environ.*, 2021, **287**, 119926.
15. L. Ning, X. Chen, Z. Wang and J. Xu, *Appl. Catal. B: Environ.*, 2023, **324**, 122282.
16. Q. Zhang, L. Jiang, J. Wang, Y. Zhu, Y. Pu and W. Dai, *Appl. Catal. B: Environ.*, 2020, **277**, 119122.
17. K. Nath, M. Chandra, D. Pradhan and K. Biradha, *ACS Appl. Mater. Interfaces*, 2018, **10**, 29417-29424.
18. Y. Chen, C. Zhang, X. Zhang, X. Ou and X. Zhang, *Chem. Commun.*, 2013, **49**, 9200-9202.

19. J. Li, S. Ding, X. Ren, Q. Sun, L. Sun, L. Zheng, F. Li, W. Zhu and W. Hu, *ACS. Mater. Lett.*, 2022, **4**, 1483-1492.
20. H. Huang, Y. Song, N. Li, D. Chen, Q. Xu, H. Li, J. He and J. Lu, *Appl. Catal. B: Environ.*, 2019, **251**, 154-161.
21. Q. Shen, L. Wei, R. Bibi, K. Wang, D. Hao, J. Zhou and N. Li, *J. Hazard. Mater.*, 2021, **413**, 125376.
22. Y. Wen, Á. Rentería-Gómez, G. S. Day, M. F. Smith, T.-H. Yan, R. O. K. Ozdemir, O. Gutierrez, V. K. Sharma, X. Ma and H.-C. Zhou, *J. Am. Chem. Soc.*, 2022, **144**, 11840-11850.
23. P. Xia, S. Cao, B. Zhu, M. Liu, M. Shi, J. Yu and Y. Zhang, *Angew. Chem. Int. Ed.*, 2020, **59**, 5218-5225.
24. Y. Guo, Q. Zhou, J. Nan, W. Shi, F. Cui and Y. Zhu, *Nat. Commun.*, 2022, **13**, 2067.
25. Q. Wu, C.-L. Cheng and T. Van Voorhis, *J. Chem. Phys.*, 2007, **127**, 164119.
26. S. R. Yost, J. Lee, M. W. B. Wilson, T. Wu, D. P. McMahon, R. R. Parkhurst, N. J. Thompson, D. N. Congreve, A. Rao, K. Johnson, M. Y. Sfeir, M. G. Bawendi, T. M. Swager, R. H. Friend, M. A. Baldo and T. Van Voorhis, *Nat. Chem.*, 2014, **6**, 492-497.
27. Z.-Q. You and C.-P. Hsu, *J. Chem. Phys.*, 2010, **133**, 074105.
28. W. J. Hehre, R. Ditchfield and J. A. Pople, *J. Chem. Phys.*, 1972, **56**, 2257-2261.
29. Y. Shao, Z. Gan, E. Epifanovsky, A. T. B. Gilbert, M. Wormit, J. Kussmann, A. W. Lange, A. Behn, J. Deng, X. Feng, D. Ghosh, M. Goldey, P. R. Horn, L. D. Jacobson, I. Kaliman, R. Z. Khaliullin, T. Kuś, A. Landau, J. Liu, E. I. Proynov, Y. M. Rhee, R. M. Richard, M. A. Rohrdanz, R. P. Steele, E. J. Sundstrom, H. L. Woodcock, P. M. Zimmerman, D. Zuev, B. Albrecht, E. Alguire, B. Austin, G. J. O. Beran, Y. A. Bernard, E. Berquist, K. Brandhorst, K. B. Bravaya, S. T. Brown, D. Casanova, C.-M. Chang, Y. Chen, S. H. Chien, K. D. Closser, D. L. Crittenden, M. Diedenhofen, R. A. DiStasio, H. Do, A. D. Dutoi, R. G. Edgar, S. Fatehi, L. Fusti-Molnar, A. Ghysels, A. Golubeva-Zadorozhnaya, J. Gomes, M. W. D. Hanson-Heine, P. H. P. Harbach, A. W. Hauser, E. G. Hohenstein, Z. C. Holden, T.-C. Jagau, H. Ji, B. Kaduk, K. Khistyaev, J. Kim, J. Kim, R. A. King, P. Klunzinger, D. Kosenkov, T. Kowalczyk, C. M. Krauter, K. U. Lao, A. D. Laurent, K. V. Lawler, S. V. Levchenko, C. Y. Lin, F. Liu, E. Livshits, R. C. Lochan, A. Luenser, P. Manohar, S. F. Manzer, S.-P. Mao, N.

Mardirossian, A. V. Marenich, S. A. Maurer, N. J. Mayhall, E. Neuscamman, C. M. Oana, R. Olivares-Amaya, D. P. O'Neill, J. A. Parkhill, T. M. Perrine, R. Peverati, A. Prociuk, D. R. Rehn, E. Rosta, N. J. Russ, S. M. Sharada, S. Sharma, D. W. Small, A. Sodt, T. Stein, D. Stück, Y.-C. Su, A. J. W. Thom, T. Tsuchimochi, V. Vanovschi, L. Vogt, O. Vydrov, T. Wang, M. A. Watson, J. Wenzel, A. White, C. F. Williams, J. Yang, S. Yeganeh, S. R. Yost, Z.-Q. You, I. Y. Zhang, X. Zhang, Y. Zhao, B. R. Brooks, G. K. L. Chan, D. M. Chipman, C. J. Cramer, W. A. Goddard, M. S. Gordon, W. J. Hehre, A. Klamt, H. F. Schaefer, M. W. Schmidt, C. D. Sherrill, D. G. Truhlar, A. Warshel, X. Xu, A. Aspuru-Guzik, R. Baer, A. T. Bell, N. A. Besley, J.-D. Chai, A. Dreuw, B. D. Dunietz, T. R. Furlani, S. R. Gwaltney, C.-P. Hsu, Y. Jung, J. Kong, D. S. Lambrecht, W. Liang, C. Ochsenfeld, V. A. Rassolov, L. V. Slipchenko, J. E. Subotnik, T. Van Voorhis, J. M. Herbert, A. I. Krylov, P. M. W. Gill and M. Head-Gordon, *Mol. Phys.*, 2015, **113**, 184-215.

30. V. Barone and M. Cossi, *J. Phys. Chem. A*, 1998, **102**, 1995-2001.
31. M. Cossi, N. Rega, G. Scalmani and V. Barone, *J. Comput. Chem.*, 2003, **24**, 669-681.
32. I. Y. Bagryanskaya, Y. V. Gatilov, E. Lork, R. Mews, M. M. Shakirov, P. G. Watson and A. V. Zibarev, *J. Fluorine Chem.*, 2002, **116**, 149-156.
33. J. Iball and J. M. Low, *Acta Crystallogr. Sect. B: Struct. Sci.*, 1974, **30**, 2203-2205.
34. A. Camerman, J. Trotter and J. M. Robertson, *Proc. R. Soc. London, Ser. A*, 1997, **279**, 129-146.
35. Y. Huang, J. Xing, Q. Gong, L.-C. Chen, G. Liu, C. Yao, Z. Wang, H.-L. Zhang, Z. Chen and Q. Zhang, *Nat. Commun.*, 2019, **10**, 169.